Journal of Sea Research 211 (2026) 102700

Contents lists available at ScienceDirect

Journal of Sea Research

journal homepage: www.elsevier.com/locate/seares

Concentration-dependent settling velocities of cohesive sediments from the Port of Hamburg based on ultrasound velocity profiling

M. Witt [a,*], J. Patzke [a], E. Nehlsen [b], P. Fröhle [a]

[a] Institute of River and Coastal Engineering (IWB), Hamburg University of Technology, Hamburg, Germany
[b] Department of Architecture and Civil Engineering, Technical University of Applied Sciences Lübeck, Lübeck, Germany

ARTICLE INFO

Keywords:
Settling
Deposition
Concentration
Cohesive
Sediment
Ultrasound
UVP
Elbe
Port of Hamburg

ABSTRACT

The settling behavior of cohesive sediments plays a key role in estuarine sediment dynamics and harbor maintenance. This study aimed to assess the applicability of Ultrasound Velocity Profiling (UVP) to capture the spatial and temporal evolution of the settling process and to derive concentration-dependent settling velocities. Laboratory experiments were conducted in a settling column with initial sediment concentrations (C_0) of 0.3–80 g/L, using cohesive sediments from the Port of Hamburg. A 4 MHz transducer was utilized to measure the vertical particle velocities with a resolution of 0.08 mm/s and a sampling volume height of 1 mm. Effective settling velocities were derived from the UVP measurements and compared to the settling velocities obtained from the lutocline evolution. Subsequently, common mathematical models were fitted to the data. The results demonstrate that UVP is a suitable, non-intrusive method for high-resolution imaging of settling processes, revealing concentration-dependent characteristics in particle movement in unprecedented detail. The calculated effective settling velocities increased approximately linearly in the flocculation settling range until a maximum of $w_{s,max}$ = 2 mm/s was reached at C_0 = 3.5 g/L, followed by an asymptotic decline in the hindered settling range. The associated deposition flux showed a broad maximum of approximately 0.01 kg/(m^{2}s) for C_0 in the range of 5–15 g/L. The results provide previously unavailable, site-specific data on the settling behavior of the studied cohesive sediments. Potential application areas of UVP include the execution of field experiments and the automated high-resolution tracking of the lutocline or bed level.

1. Introduction

The settling velocity of cohesive sediments is a key parameter for understanding and modeling sediment dynamics in estuarine and coastal systems. Since this parameter is highly site-specific and the processes underlying the settling and deposition of cohesive sediments are not yet fully understood, there is a need for straightforward field and laboratory methods to investigate and quantify it.

The settling velocity of cohesive sediment flocs is primarily controlled by their properties like size, density and shape (Winterwerp et al., 2021). A given volume usually contains a large number of flocs with different settling velocities. A common simplification is therefore to describe the total population by a characteristic or effective settling velocity w_s (e.g., Pejrup and Mikkelsen (2010)). Unless otherwise specified, the term "settling velocity" in this work always refers to this characteristic value. Since in natural environments flocs are constantly in a transient state of formation and breakup, their bulk properties are strongly influenced by the frequency of interparticle collisions. As the collision frequency is dependent on the particle concentration, the suspended sediment concentration (SSC) is commonly used as an aggregate parameter to approximate the effective settling velocity (Mehta and McAnally, 2008). Many field and laboratory studies investigated the settling velocity of cohesive sediments in relation to the suspended sediment concentration (Odd and Rodger, 1986; Ross, 1988; Delo and Ockenden, 1992; Wolanski et al., 1992). Both field and laboratory experiments show an increase of the settling velocity for increasing sediment concentrations up to a threshold in the range of SSC = 1–10 g/L, what is often termed flocculation settling (cf. Fig. 1A). For higher sediment concentrations, the settling velocities decrease again due to the increasing effects of the upward directed return flow of water. This is referred to as hindered settling. Fig. 1B illustrates the temporal evolution of a settling experiment in a settling column in the hindered settling regime after homogenization. Characteristic features are the formation of a lutocline, a sediment formation line and a settling zone of virtually

* Corresponding author.
E-mail address: markus.witt@tuhh.de (M. Witt).

https://doi.org/10.1016/j.seares.2026.102700
Received 14 January 2026; Received in revised form 12 March 2026; Accepted 13 April 2026
Available online 15 April 2026

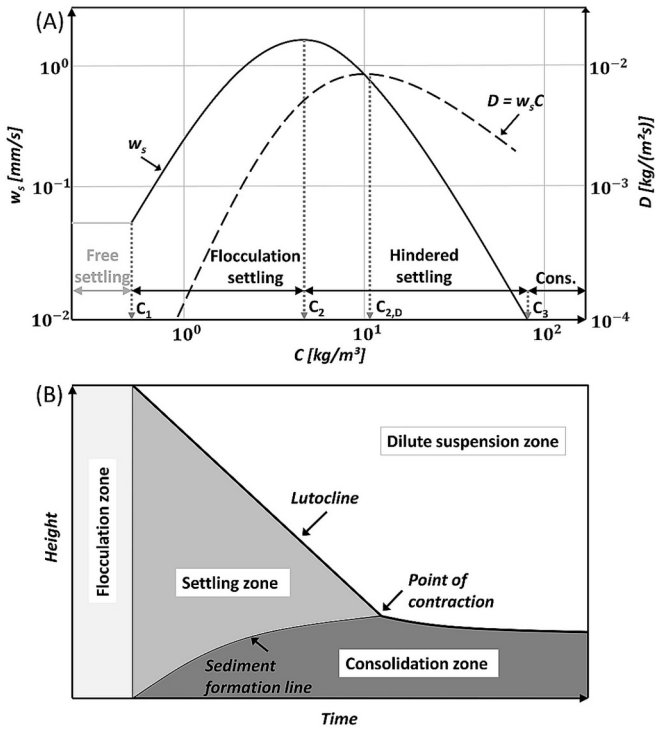

Fig. 1. A) Schematic relation between sediment concentration and effective settling velocity (adapted from Mehta and McAnally (2008)); B) Illustration of the settling process in a settling column for suspensions in the hindered settling range (adapted from Imai (1981)).

constant sediment concentration and settling velocity (Kynch, 1952; Imai, 1981). Once the SSC exceeds a critical value, the flocs interconnect to form a continuous network. This is called the gelling point and is commonly seen as transition between suspension and (soft) sediment bed, or between settling and consolidation. The gelling concentration is reported to be in the range of SSC = 20–120 g/L (Dankers, 2006; Papenmeier, 2012; te Slaa, 2020).

Different mathematical models for the prediction of the settling velocity of cohesive sediments in relation to the sediment concentration were proposed. One widely used empirical approach for the range of flocculation settling is a simple power-law formulation reading (van Leussen, 1994; Whitehouse et al., 2000):

$$w_s = kC^n \tag{1}$$

herein, w_s expresses the effective settling velocity [m/s], C [kg/m^3] is the sediment concentration and k as well as n are empirical parameters, which need to be fitted on experimental data. For the range of hindered settling, Winterwerp (1999) proposed a semi-empirical model, which is based on the approach of Richardson and Zaki (1954). The formulation of Winterwerp (1999) accounts for viscosity and return flow effects and has the form:

$$w_s = w_{s,r}\frac{(1-\phi)^m(1-\phi_s)}{1+2.5\phi} \tag{2}$$

with $w_{s,r}$ as reference settling velocity of a single mud floc in still water [m/s]. The solid volume fraction is calculated as $\phi_s = C/\rho_s$ [−], with ρ_s as density of the sediment particles [kg/m^3]. The parameter $\phi = C/C_{gel}$ [−] describes the actual sediment concentration in relation to the gelling concentration. The value of the exponent m is usually set to $m = 2$ (Winterwerp et al., 2021). By substituting $w_{s,r}$ in Eq. (2) with w_s from Eq. (1), a continuous formulation applicable for both flocculation settling and hindered settling is obtained (Weilbeer (2008)).

Another model which is supposed to cover the whole range of flocculation settling as well as hindered settling was proposed by Wolanski et al. (1989). The original model was further generalized in Mehta (2014) and reads:

$$w_s = a_w\frac{C^{n_w}}{\left(C^2+b_w^2\right)^{m_w}} \tag{3}$$

herein, a_w may be interpreted as settling velocity scaling coefficient, n_w as flocculation settling exponent and b_w, m_w as hindered settling coefficient and exponent, respectively. All these empirical parameters need to be calibrated based on experimental data.

Ultrasound velocity profiling (UVP) was introduced to the field of fluid mechanics by Takeda (1986) and has been successfully applied to study multiphase flows in pipes and free surface channels since then (e.g. Wiklund and Stading (2008), Pedocchi and García (2012), Hitomi et al. (2021)). In UVP, velocity profiles along an ultrasound beam are calculated by analyzing the backscattered echo of suspended particles (see Section 2.2). The main advantages of the UVP technique are the non-intrusive application, the capability to measure in opaque suspensions and the high spatial and temporal resolution. The particle type and the flow conditions are typically chosen to prevent settling due to particle weight, ensuring that the particles move with the flow and allowing the particle motion to directly reflect the velocity field. Hunter et al. (2011) instead showed that UVP may also be used to investigate the settling process of the particles itself. They used coagulated and non-coagulated glass particles for their experiments in a settling column under quiescent conditions and settling velocities were successfully measured, despite the relatively low velocity resolution applied. Patzke (2025) conducted comparable experiments with natural cohesive sediments and laid the foundation for the present work. In the present study, the experimental procedure, the settings of the UVP device and the processing of the measurement data have been further improved. Traditional methods for determining the settling velocity of cohesive sediments are typically based on visual tracking of the lutocline in settling columns, optical measurements, or indirect estimates from concentration profiles (Winterwerp and van Kesteren, 2004; Mantovanelli and Ridd, 2006). These approaches often provide limited spatial or temporal resolution and may be affected by the opacity of the suspension. In contrast, UVP offers the potential to resolve the internal velocity structure of the settling suspension and to capture the settling process continuously in space and time. The novelty of the present study therefore lies in the systematic and optimized application of UVP to investigate the settling behavior of natural cohesive sediments and to obtain high-resolution information on concentration-dependent settling dynamics.

The aims of this study are to:

- Examine the applicability of UVP as a non-intrusive technique to study the settling process of cohesive sediments over a wide range of concentrations.
- Derive effective settling velocities from the measurement data.
- Analyze the influence of the suspended sediment concentration on the settling velocity and fit existing mathematical models to the data.

2. Material and methods

2.1. Sampling site and sediment properties

The sediment used for the experiments was collected in the Elbe in the area of the Port of Hamburg in August 2024. Sampling was conducted using a van Veen grab sampler in the semi-enclosed, hydrodynamically sheltered side channel “Köhlfleet”, which is a known sedimentation hotspot (Fig. 2). Especially during periods of low river discharge of the Elbe, the upstream limit of the turbidity zone of the Elbe estuary shifts toward the Port of Hamburg and leads to increased suspended sediment concentrations (Weilbeer et al., 2021). As the “Köhlfleet” is located at the western end of the Port of Hamburg, the

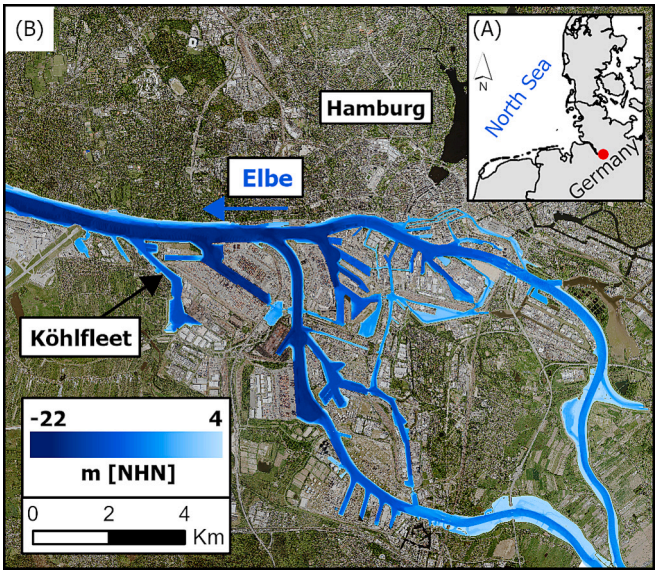

Fig. 2. Sampling site „Köhlfleet" in the area of the Port of Hamburg. The red dot in panel A indicates the location of the Port of Hamburg. (Bed-level data: WSV (2024); background image: LGV (2024)).

turbidity zone reaches it prior to other parts of the harbor and the low-energy conditions foster sedimentation, comparable to a harbor basin. The sediment sample was stored in an airtight, optically opaque container in a cooling unit.

The grain size distribution of the sample was derived by a combined sieve and hydrometer analysis following ISO 17892-4 (DIN, 2017). For the sieve analysis (diameter (D) > 63 µm), the sample was dried at 105 °C, whereas the hydrometer analysis was conducted using the wet sample. The clay content was 33% (D < 2 µm), the silt content was 64% (2 µm < D < 63 µm) and the fine sand content was 3% (D > 63 µm), leading to a median diameter D_{50} of 8 µm. Additionally, the particle volume distribution was measured in a dispersed and a flocculated state with a Malvern Mastersizer 3000 to obtain an indication of the floc sizes formed by the sediment sample (Fig. 3). For the dispersed state $D_{50,V}$ = 13 µm and for the flocculated state $D_{50,V}$ = 74 µm was derived. The curve shown for the flocculated state corresponds to a sample of C_0 = 1 g/L at a shear rate of G = 50 1/s, after reaching equilibrium. Shear rates of this magnitude may lead to partial floc breakup (van Leussen, 1994). However, lower shear rates were not feasible during the flocculation tests, as the suspension had to be continuously pumped through the measuring unit, imposing

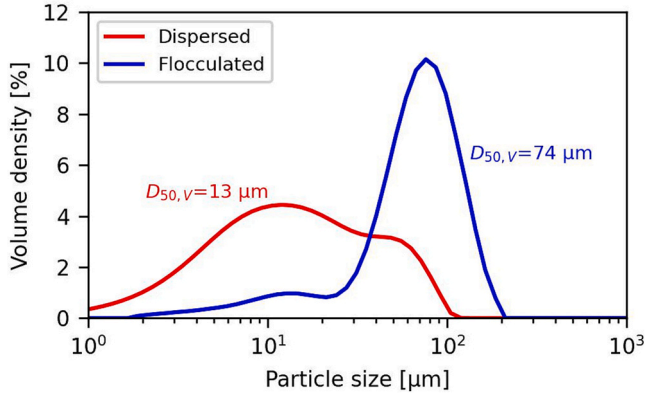

Fig. 3. Volume distribution of particle sizes measured in a Malvern Mastersizer 3000 in dispersed state and flocculated state for the utilized sediment sample. The flocculated state corresponds to the equilibrium state reached at C_0 = 1 g/L and G = 50 1/s.

corresponding shear rates within the tubing. Since the shear rates in the conducted settling column experiments were much lower after reaching quiescent conditions, the floc size distribution may have been shifted toward even larger floc sizes. For concentrations of 5 g/L and 20 g/L, $D_{50,V}$ values of 47 µm and 32 µm, respectively, were measured in the flocculated state, indicating decreasing floc sizes with increasing C_0. This trend may be attributed to increasing mutual hindrance between particles in this concentration range (Whitehouse et al., 2000). The differences between the Mastersizer's laser diffraction analysis for the dispersed state and the hydrometer analysis are due to the respective measurement principles and target values. In van Rijn et al. (2025) these differences are discussed in detail and comparable deviations of D_{50} and $D_{50,V}$ are reported. The loss on ignition (LOI) was determined following EN 17685-1 (DIN, 2023) by annealing at 550 °C and provides an approximation of the total organic content of the sample. The LOI was measured as 12%.

In addition to the sediment, site-specific water was collected for the laboratory experiments. The salinity was 0.4 PSU, indicating freshwater conditions close to the freshwater-brackish transition. The speed of sound (c) was 1475 m/s at room temperature of 18 °C.

2.2. Ultrasound velocity profiling and DOP3010 device

Ultrasound Velocity Profiling (UVP) is an acoustic technique used to measure velocity profiles in fluids by analyzing the backscattered echoes from suspended particles. Unlike continuous-wave Doppler methods, UVP systems operate in a pulsed mode: short ultrasonic bursts are transmitted into the medium, and the echoes returning from scatterers are recorded as a function of time. Therefore, the technique is also referred to as Pulsed Ultrasound Velocimetry (PUV). The travel time of the echo provides the depth (d [m]) information of the sampling volume:

$$d = c\frac{\Delta T}{2} \tag{4}$$

with c [m/s] as the speed of sound and ΔT [s] as time difference between emission and reception of the echo. To calculate the velocity of the moving particles the phase shift between successive echoes is evaluated and converted to a frequency shift, which allows the application of the Doppler equation:

$$v = \frac{cf_D}{2f_E cos(\delta)} \tag{5}$$

herein, v [m/s] is the velocity of the particles relative to the ultrasonic beam axis, f_D [1/s] the Doppler frequency shift, f_E [1/s] the frequency of the emitted signal and δ [rad] the potential angle between the beam axis and the mean direction of particle motion.

Since a single sampling volume contains numerous particles moving at different velocities, the received acoustic signal represents a spectrum of Doppler frequencies. The signal is subsequently filtered and decomposed, allowing the individual velocity components contributing to this spectrum to be isolated. A characteristic mean velocity v_m is then obtained by computing the spectral-intensity-weighted average across all velocity bins, accounting for their respective contributions to the overall signal (Fig. 4). This provides a representative estimate of the particle velocity within the sampling volume. Implications of this assumption are discussed in Section 4.

The maximum detectable particle velocity (v_{max}) is given by the Nyquist-Shannon sampling theorem as:

$$v_{max} = \frac{cf_{PRF}}{4f_E cos(\delta)} \tag{6}$$

with f_{PRF} [1/s] as pulse repetition frequency. Phase shifts leading to velocities above this threshold are misinterpreted, and the calculated velocities are folded back into the low/negative velocity range. This effect is called aliasing. Additional information on the working principles of UVP can be found in Takeda (1991), Takeda (1995), Poelma

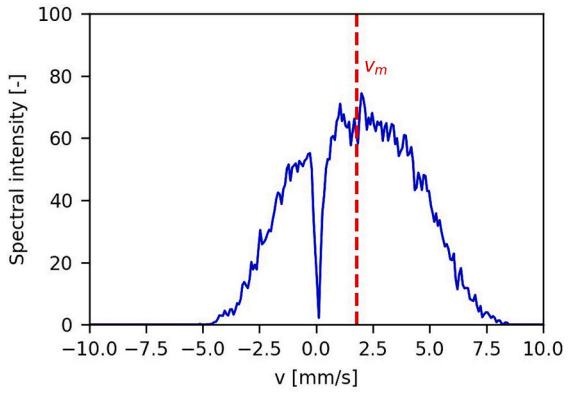

Fig. 4. Example of a power spectrum obtained from a sampling volume. The spectrum corresponds to a sampling volume at a depth of 30 cm in an experiment with $C_0 = 4$ g/L, and was averaged over $T = 150$–240 s. Spectral intensity is expressed in arbitrary units. The zero intensity at $v = 0$ mm/s results from high-pass filtering applied before the spectrum was computed by the DOP3010.

(2017) and Hoskins et al. (2010).

For the UVP measurements conducted in the present study, a Signal Processing DOP3010 device (Signal Processing S.A., 2025) was utilized with a 4 MHz transducer, which had an outer diameter of 8 mm containing a piezoelectric element with a diameter of 5 mm. Both the emitting frequency and the piezoelectric element diameter govern the extent of the ultrasonic beam perpendicular to the beam axis. For the given parameters, the near field, in which the acoustic field is approximately cylindrical with a diameter close to that of the emitter, had a length of ~1.7 cm. In the far field (> 1.7 cm distance to the transducer) the beam spread with an effective half angle β of 2.2° (cf. Signal Processing S.A. (2025)). This effective half angle corresponds to the −6 dB beam boundary, where the acoustic intensity is reduced to 25% of its on-axis value. Table 1 summarizes the settings of the DOP3010 and additional parameters used in the UVP measurements.

2.3. Experimental setup and procedure

The basic experimental setup is illustrated in Fig. 5. It consisted of an acrylic column with a width of 20 cm and a height of 70 cm, which was filled with a water–sediment suspension to a height of 50 cm, resulting in a suspension volume of 15.7 L. Following homogenization (see the next paragraph), a top plug was inserted into the column to accurately position the ultrasound transducer along the central axis. The transducer extended 2 cm below the foam plug to ensure continuous contact with the suspension and was connected to the DOP3010 controller, which was in turn connected to a computer running the UDOP software package. In this configuration, the ultrasound beam axis coincided with the direction of particle settling.

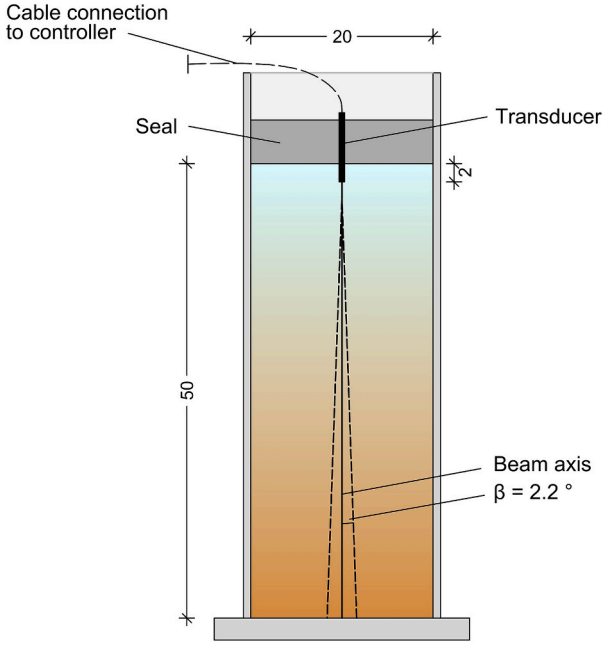

Fig. 5. Schematic outline of the experimental setup. Length specifications are in cm.

To investigate the influence of the initial sediment concentration (C_0) on settling behavior and settling velocity, C_0 was increased incrementally in successive experiments within each experimental run (see Table 2 for an overview of the conducted experiments). In the first experiment of a run, sediment was added until an initial concentration of $C_0 = 0.3$ g/L was reached. This value is reported in the literature as the lower boundary for flocculation settling (Mehta, 2014), and preliminary tests showed that no reliable results were obtained below this concentration due to large scatter. The suspension was homogenized in a standardized manner by stirring for 1 min using a high-torque hand mixer equipped with a helical ribbon impeller with a diameter of 14 cm. The high shear rates applied during homogenization additionally caused floc breakup. After homogenization was completed, a thin metal plate with a width matching the inner diameter of the settling column was inserted into the column for 5 s to suppress the rotational flow and was then carefully removed. Subsequently, the top plug carrying the transducer was positioned in the column. The start of the UVP measurement, defined as $T = 0$ s, was set to 1 min after the end of the homogenization process. The standard measurement duration was 6 min, as a substantial part of the initially suspended sediment had deposited at the column bottom within this time. For selected experiments, the measurement duration was extended to up to 60 min to investigate processes occurring over longer timescales and to assess the capability of the applied method

Table 1
Parameters and settings of the DOP3010 used for the UVP measurements.

Parameter	Value	Description
Emitting frequency (f_E)	4 MHz	
Pulse repetition period (PRP)	9.3 ms	Corresponding to a pulse repetition frequency (f_{PRF}) of ~108 Hz
Emissions per profile	20	Number of consecutive pulses from which one velocity profile is calculated
Velocity profile output interval	345 ms	(PRP * Emissions per profile) + time for internal data processing and transmission
Velocity scale (v_{max})	± 10 mm/s	see Eq. (6)
Velocity resolution	0.078 mm/s	The velocity range is divided into 256 discrete bins
First gate depth	10 mm	
Spatial resolution/Vertical extent of sampling volumes	1.1 mm	Spatial resolution (distance between discrete output points) and vertical extent of sampling volumes are equal, preventing overlap between sampling volumes
Speed of sound	1475 m/s	
Doppler angle (δ)	0°	Transducer positioned in the main direction of particle movement
Signal amplification (TGC)	40 dB	Uniform value, independent of the distance to the transducer

Table 2
Overview of the conducted experiments.

	SSC-range [g/L]	Measurement techniques	Total number of experiments
Run 1	0.3–20	UVP	46
	20–30	UVP and photographic evaluation of lutocline	
	30–80	photographic evaluation of lutocline	5
Run 2	0.3–10	UVP	18
Repeatability tests	0.5–10	UVP	20

to capture these effects. After completion of each experiment, the suspended sediment concentration was increased and the procedure was repeated. The step size of the concentration increase was adjusted in relation to the total SSC and ranged from $\Delta SSC \cong 0.05$ g/L at total SSC < 1 g/L and $\Delta SSC \cong 2.5$ g/L for total SSC > 20 g/L.

SSC measurements were performed using both an optical Hach Solitax hs-line sc probe, which was pre-calibrated for the internal conversion of turbidity to SSC, and an Anton Paar DMA 35 density meter. The two devices showed good agreement, with a mean deviation of approximately 5% for SSC values between 0.3 and 30 g/L. For SSC < 5 g/L, data from the optical probe were used, whereas for SSC ≥ 5 g/L data from the density meter were applied, as the respective measurement principle excels in this concentration range.

2.4. Calculation of concentration-dependent settling velocities

To obtain concentration-dependent effective settling velocities w_s, the particle velocity v_m recorded by the DOP3010 for each sampling volume was further averaged over a defined depth interval of the settling column and a specified time period for each experiment (Fig. 6).

For initial sediment concentrations $C_0 < 2.5$ g/L, no distinct settling zone could be identified. To maximize the amount of data included in the averaging procedure for this range of concentrations, the depth interval was therefore set to 10–48 cm and the time window to $T =$ 150–330 s. The initial period up to 150 s was excluded to avoid the influence of the homogenization process. Time intervals beyond 330 s and depths under 10 cm were excluded to account for ongoing particle settling and regions in which the assumption of an approximately homogeneous sediment concentration may no longer be valid.

For $C_0 \geq 2.5$ g/L, a progressively more distinct settling zone was observed. Within this zone, the sediment concentration is approximately homogeneous and equal to the initial sediment concentration (Kynch, 1952). The corresponding settling velocities were calculated as the mean of the data contained within the rectangles illustrated in Fig. 6D-I. These rectangles span a time interval from $T = 150$–240 s and are bounded by the lutocline above and the sediment formation line below along the depth axis. If no sediment formation line was discernible due to limited ultrasound penetration at high concentrations ($C_0 > \sim 20$ g/L), the non-penetrated lower section of the column was excluded from the analysis.

As a lutocline was detected in all UVP measurements for $C_0 \geq 2.5$ g/

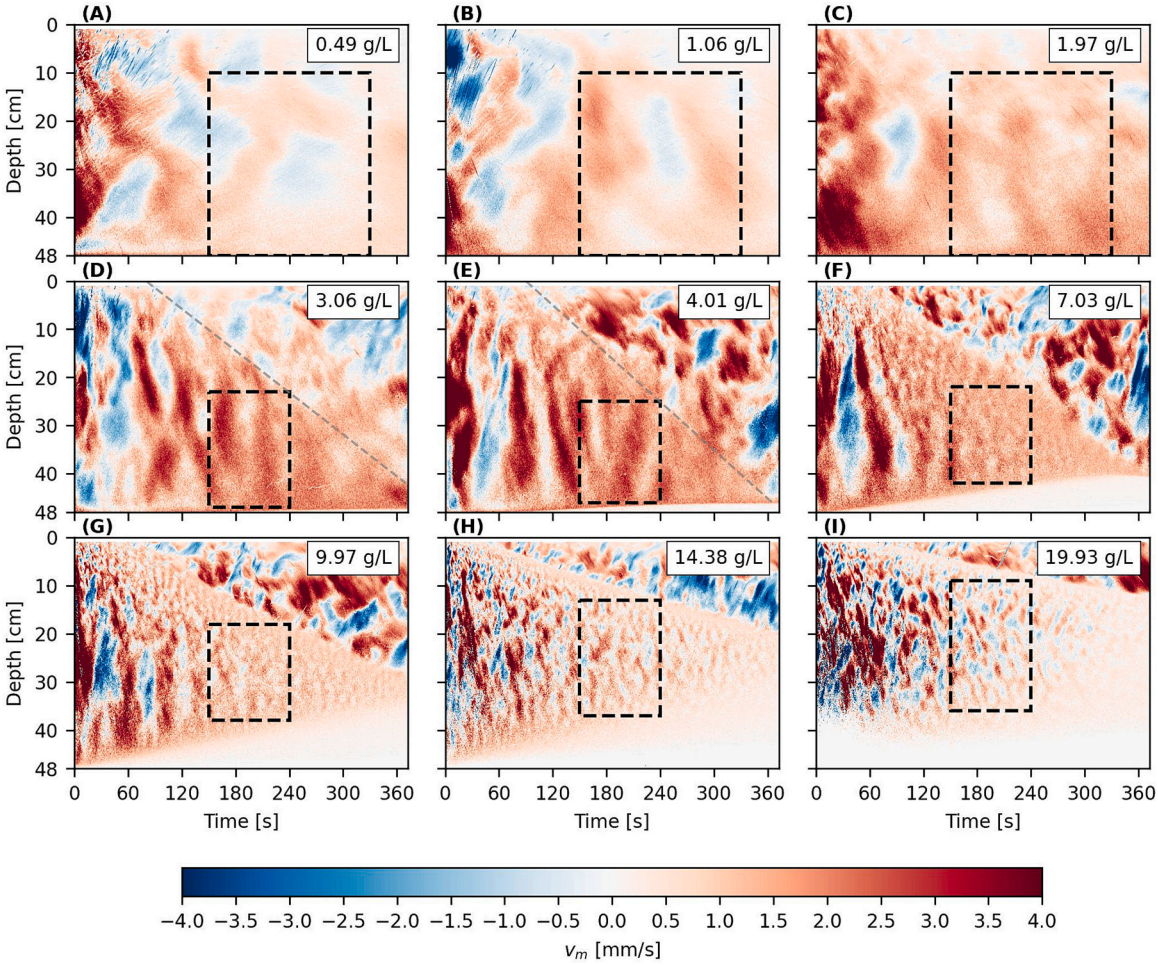

Fig. 6. Measured vertical particle velocities in the settling column over depth and time. Downward directed velocities are shown as positive values (red), upward directed velocities as negative values (blue). The initial concentration of each experiment is shown on the top right. The marked boxes indicate the values over which was averaged to determine w_s. In panels D-E, the emerging boundary between the settling zone and the dilute suspension zone is highlighted by a gray dashed line.

L, settling velocities were additionally derived from the slope of the lutocline. The results obtained from both approaches were compared for mutual validation and to assess the consistency of the measurement data. For initial sediment concentrations above 20 g/L, the lutocline was sufficiently sharp to be unambiguously identified by visual inspection of the settling column. Photographs were taken at regular intervals, from which the settling velocity of the lutocline was determined. This approach allowed, on the one hand, verification of the agreement between the UVP-derived velocities and visual observations and, on the other hand, extension of the investigated SSC range to concentrations for which the applied UVP setup was no longer applicable (see Table 2).

3. Results

3.1. Temporal evolution of the settling process

The temporal evolution of the settling process as captured by UVP is illustrated in Fig. 6 for different initial sediment concentrations. In all experiments shown, decaying turbulent fluctuations were observed during approximately the first 150 s of the measurements, representing remains of the homogenization process. After the homogenization-induced turbulence had dissipated, particles in the suspension generally settled along the beam axis. However, the characteristics of the observed particle motion differed substantially depending on the initial sediment concentration.

Fig. 6A-C shows the resulting particle motion for initial sediment concentrations up to 2 g/L. In this concentration range, no distinct settling zone was formed. Overall, the magnitude of the mean particle velocity v_m increased with increasing sediment concentration, while regions of slightly upward-directed particle motion became progressively less pronounced. Although turbulence damping generally increases with sediment concentration and may influence the time required for dissipation of homogenization-induced turbulence, it cannot explain the observed trend in v_m. Instead of a reduction in velocity fluctuations, the data indicate a systematic shift of the entire velocity distribution toward higher downward-directed values with increasing C_0.

From an initial concentration of 3 g/L onward (Fig. 6D-F), a progressively clearer separation became apparent between a lower section with virtually homogeneous settling velocities and an upper section dominated by random turbulent structures. This pattern corresponds to the formation of a settling zone and a dilute suspension zone, as illustrated in Fig. 1B. Although the lutocline could be clearly identified in the ultrasound measurement data at initial concentrations of only a few grams per liter, visual observations during the experiments showed that the transition zone still had a vertical extent of several centimeters at these concentrations. With increasing initial concentration, the transition became sharper, and at $C_0 \cong$ 20 g/L the lutocline position could be determined visually with a precision of ±1 mm (Fig. 7). The measured v_m in the settling zone generally decreased with increasing initial concentration. For $C_0 \geq \sim$10 g/L, small-scale patterns of alternating upward and downward particle motion developed within the settling zone (Fig. 6G-I). This behavior was also confirmed by visual observations: transient clouds of particles formed that either settled downward or were transported upward by the return flow, indicating markedly turbulent conditions. At the bottom of the column, a bed layer of increasing thickness formed as sediment deposited (Fig. 6D-H). Within this bed layer, particles formed a continuous network and individual particle motion was no longer observable. Because the layer as a whole underwent consolidation, during which vertical particle motion is much slower than during settling, it appeared as zero values in the measurements. From $C_0 \cong$ 20 g/L onward, the ultrasound signal no longer penetrated the full column depth (see Fig. 6I). Viable measurements were obtained up to $C_0 = 30$ g/L. Above this concentration, the penetration depth became too low and the measurement data were no longer reasonable.

Fig. 8 shows the results of the UVP measurements for an initial sediment concentration of 10.1 g/L over an extended measurement

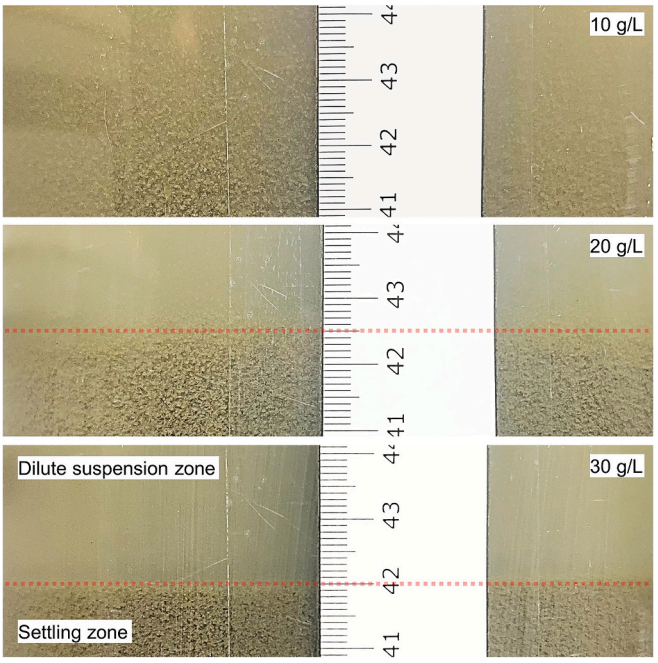

Fig. 7. Sharpening of the transition between the dilute suspension zone and the settling zone with increasing initial sediment concentration. The corresponding concentrations are given in the top right corner. The position of the lutocline for $C_0 = 20$ g/L and $C_0 = 30$ g/L is indicated by a red dotted line.

period of 20 min. As in Fig. 6D-H, both the settling zone and the bed layer are clearly identifiable. In addition, the echo amplitude received by the transducer at four selected points in time is illustrated, from which qualitative information can be derived. To reduce noise, a moving average over a period of 5 s was applied. The echo amplitude profiles exhibited an approximately exponential decrease with depth within each zone in the settling column, consistent with theory for a constant signal amplification level in a homogeneous medium (Ainslie, 2010). In the dilute suspension zone, the echo amplitude also decreased with time, indicating the ongoing reduction of sediment concentration due to settling. At the interface between the dilute suspension zone and the settling zone, as well as between the dilute suspension zone and the bed layer, a peak in echo amplitude was observed. This reflection resulted from the contrast in acoustic impedance between the adjacent zones. The peak was relatively broad at $T = 100$ s and $T = 300$ s, reflecting the diffuse boundary between the dilute suspension zone and the settling zone at the given initial sediment concentration. In contrast, a sharp boundary existed between the bed layer and the dilute suspension zone, leading to a more pronounced echo-amplitude peak at $T = 600$ s and $T =$ 1000 s. At the sediment formation line, no distinct peak in echo amplitude was identified.

Fig. 8 further illustrates that turbulence in the dilute suspension zone diminished with time. This behavior was observed in all experiments with extended measurement durations. The relatively strong turbulence present in this layer during the settling phase was likely primarily induced by the upward-directed return flow from the settling zone. During the early stage of the consolidation phase, turbulence decreased markedly as drainage rates of pore water from the bed became much lower. Nevertheless, even after 60 min of experimental duration, some velocity fluctuations were still observed. These were presumably convective flows, induced by small gradients in sediment concentration and temperature, as well as by the ongoing settling of particles. Comparable observations have been reported in the literature (e.g. van Leussen (1994)). The results demonstrate that even under laboratory conditions, the settling process of cohesive sediments is never truly "quiescent".

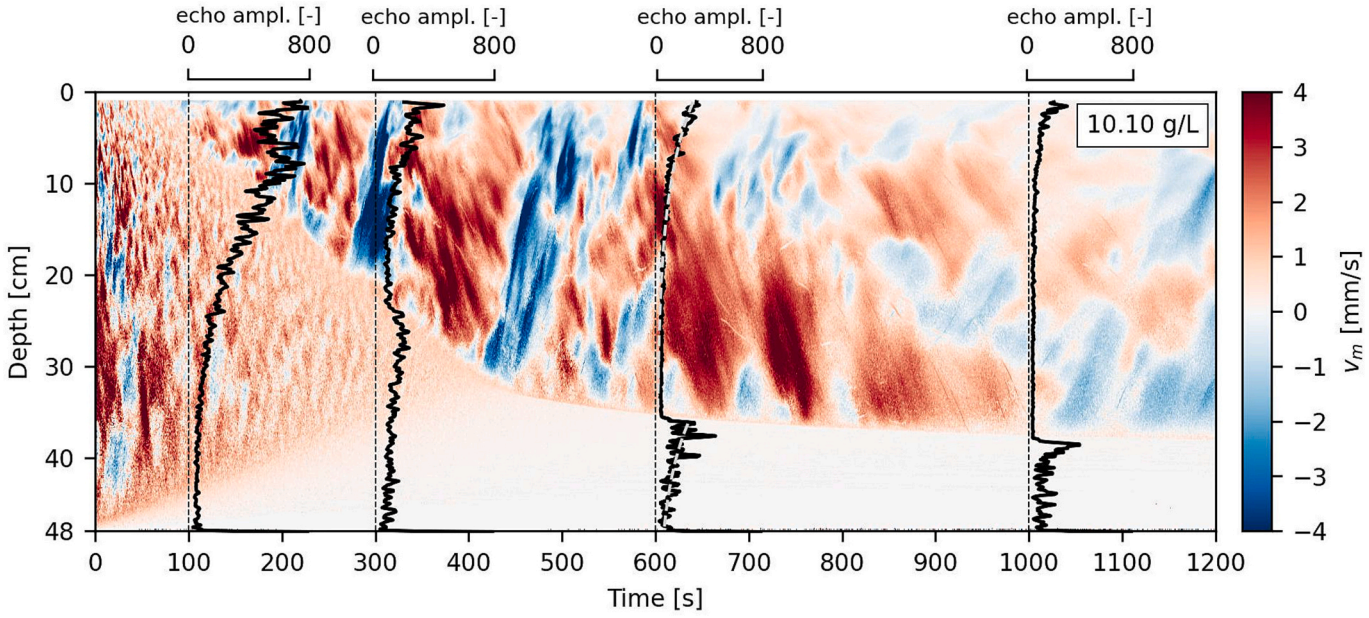

Fig. 8. Measured vertical particle velocities over depth and time for an initial sediment concentration of 10.1 g/L. Downward directed velocities are shown as positive values (red), upward directed velocities as negative values (blue). The profile of the echo amplitude received by the transducer is illustrated for four distinct points in time. Dashed gray lines for $T = 600$ s indicate exponential fits of the form $A(z) = A_0 e^{-\alpha z}$ applied separately to the regions above and below the lutocline.

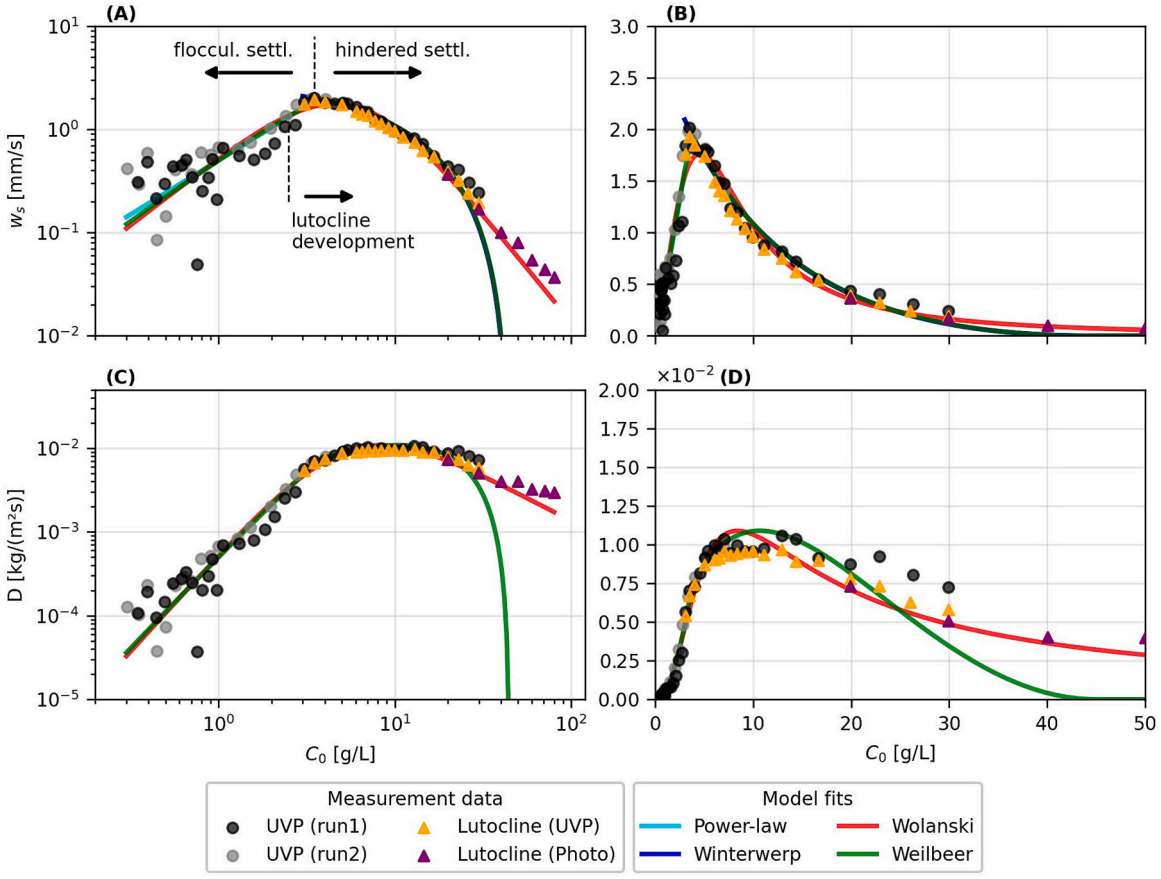

Fig. 9. A-B): Concentration-dependent settling velocities shown on logarithmic (A) and linear (B) scales. C-D): Concentration-dependent settling fluxes on logarithmic (C) and linear (D) scales. In addition, fitted mathematical models are shown (top: all; bottom: only Weilbeer (2008) and Wolanski et al. (1989) for improved readability). The models were fitted to the settling velocities derived from the UVP particle velocity data of both experimental runs (0.3 g/L $< C_0 <$ 30 g/L). Lutocline-based estimates were not included in the fit.

3.2. Concentration-dependent effective settling velocities and settling fluxes

Fig. 9A-B shows the concentration-dependent settling velocities derived as described in Section 2.4. The results are presented on both logarithmic and linear axes to reveal details across the full data range and to facilitate interpretation. For initial sediment concentrations $C_0 <$ 3.5 g/L, the calculated settling velocities increased approximately linearly with increasing initial concentration, corresponding to the flocculation settling range (cf. Fig. 1A). Despite the change in the evaluation procedure associated with the development of a lutocline for $C_0 > 2.5$ g/L, a smooth transition in the calculated settling velocities was obtained. Within the flocculation settling range, the spread of the data decreased with increasing C_0, consistent with the observations shown in Fig. 6A-C. This reduction in scatter may be attributed both to increased turbulence damping and to a decreasing ratio between unavoidable velocity fluctuations and the mean downward-directed particle velocity. At $C_0 = 3.5$ g/L, a maximum settling velocity of $w_{s,max} = 2$ mm/s was reached. The measured maxima were $w_{s,max} = 2.01$ mm/s at $C_0 = 3.48$ g/L for run 1 and $w_{s,max} = 1.98$ mm/s at $C_0 = 3.37$ g/L for run 2. For initial concentrations above of 3.5 g/L, the experiments fell within the hindered settling regime, which was reflected by continuously decreasing settling velocities. Fig. 9C-D show the settling flux D, calculated from the settling velocity as $D = w_s C_0$. The settling flux increased with initial sediment concentration until it reaching a plateau for 5 g/L $< C_0 <$ 15 g/L, with values of D $\cong$ 0.01 kg/(m^{2}s). This plateau implies an inverse relationship between w_s and C_0 within this concentration range. At higher initial concentrations, the settling flux decreased again.

The settling velocities calculated directly from the UVP particle velocity data and those derived from the slope of the lutocline identified in the visualized UVP data were in close agreement. This agreement confirms the theoretical consistency of both approaches and indicates the reliability of the particle velocities measured by the UVP system. Only for $C_0 > 20$ g/L, a slight tendency toward higher settling velocities derived directly from the particle velocity data was observed, which may be attributed to the proximity to the operational limits of the DOP3010 under the applied settings. It should be noted that differences in w_s are amplified by the corresponding values of C_0 in Fig. 9C-D. The photographic evaluation of the lutocline for $C_0 > 20$ g/L was consistent with the UVP-based approaches and extended the data set up to $C_0 = 80$ g/L.

3.3. Fitting of mathematical models

The mathematical models for the calculation of w_s described in Section 1 were fitted to the settling velocities derived from the UVP particle velocity data. The best-fit parameters, determined using a least-squares approach, are summarized in Table 3, and the fitted models are visualized in Fig. 9A-B. The deposition flux shown in Fig. 9C-D was calculated by multiplying the model-derived settling velocities by C_0. For the model of Weilbeer (2008), the reference settling velocity $w_{s,r}$ was calculated from the power-law formulation given in Eq. (1). To obtain reasonable results and to limit the influence of this parameter to the flocculation settling regime, a maximum value of $w_{s,r} = 2.81$ mm/s was defined. This value corresponds to the reference settling velocity obtained from fitting the model of Winterwerp (1999) to the data.

All fitted models reproduced the overall trend of the measurement data to a high degree. Since the Weilbeer model is composed of the power-law approach for the flocculation settling regime and the Winterwerp model for the hindered settling regime, the model curves are nearly congruent within the respective concentration ranges. However, the composite model is capable of providing a smooth transition between the two regimes. When comparing the models of Weilbeer and Wolanski, notable deviations occurred for initial sediment concentrations $C_0 > 30$ g/L. Extending the data range for model fitting to initial sediment concentrations of up to 80 g/L by including photographic lutocline data had virtually no influence on the derived best-fit parameters (see Table 3). This behavior may be partly attributed to the fitting procedure, which is sensitive to both data density and the magnitude of absolute errors, but primarily reflects differences in the mathematical structure of the model formulations. While the Weilbeer model predicts a settling velocity of zero at $C_0 = C_{gel}$, the Wolanski model approaches this value asymptotically. Manually imposing a higher value for C_{gel} resulted in a substantially poorer fit of the Weilbeer model in other concentration ranges.

With respect to the upper limit of the initial sediment concentrations investigated, the Wolanski model showed the best agreement with the measurement data (cf. Fig. 9). However, the exact initial sediment concentration at which the settling process transitions into a consolidation process remains unclear. Which model performs best in a higher-level hydro-morphodynamic model of e.g. an estuary will depend largely on how the transition from a highly concentrated suspension to a sediment bed is implemented, respectively how the settling velocity formulation is embedded into other submodels or holistic approaches (e.g. Kaveh and Malcherek (2024)).

Whitehouse et al. (2000), Pejrup and Mikkelsen (2010) and Mehta (2014) summarized best-fit parameters for the power-law approach (Eq. (1)) and the Wolanski model, derived from field and laboratory investigations of settling velocities of cohesive sediments from various other estuaries. The parameters obtained for sediments from the Port of Hamburg in the present study were in good agreement with ranges reported in the literature, as were the reference settling velocity and gelling concentration derived for the Winterwerp model.

3.4. Repeatability and sensitivity

The good repeatability of the results was already evident from the close agreement between the outcomes of experimental runs 1 and 2. To

Table 3
Overview of the derived best-fit parameters for the mathematical models described in Section 1. The parameters correspond to settling velocities w_s [mm/s] as a function of C_0 [kg/m^3]. Model fits were performed based on the settling velocities derived from the UVP particle velocity data. For the Winterwerp (1999) model, the parameter m was fixed at $m = 2$. RMSE denotes the root mean squared error. The upper limits of the C_0 ranges (3.5 g/L and 30 g/L) correspond to the transition between flocculation settling and hindered settling and to the maximum initial sediment concentration for which UVP measurements were feasible. (*): For $C_0 > 30$ g/L, the UVP dataset was extended using settling velocities derived from the photographic evaluation of the lutocline.

Model	C_0	Best-fit parameters								RMSE
		k	n	$w_{s,r}$	C_{gel}	a_w	b_w	n_w	m_w	
	[g/L]	[−]	[−]	[mm/s]	[g/L]	[−]	[−]	[−]	[−]	[mm/s]
Power-law	0.3–3.5	0.50	1.05	–	–	–	–	–	–	0.20
Winterwerp (1999)	3.5–30	–	–	2.81	44.63	–	–	–	–	0.08
Weilbeer (2008)	0.3–30	0.55	1.24	–	44.91	–	–	–	–	0.17
	0.3–80*	0.55	1.24		44.95					0.17
Wolanski et al. (1989)	0.3–30	–	–	–	–	223.64	5.78	1.32	1.72	0.19
	0.3–80*					212.39	5.75	1.33	1.71	0.19

further assess the repeatability and sensitivity of the UVP-based settling velocity measurements, additional experiments and analyses were conducted. Fig. 10A shows the results of repetition experiments for four different initial sediment concentrations, each based on five repetitions. Both the mean settling velocities and their trends with respect to the initial sediment concentration were consistent with the findings shown in Fig. 9. The standard deviation and range of the derived settling velocities were comparatively large for $C_0 = 0.5$ g/L and $C_0 = 1$ g/L, reflecting weak turbulence damping and particle motion that was influenced by random flow structures (Fig. 6A-C). Comparable scatter in settling velocity measurements at low initial concentrations has been reported in other field and laboratory studies and appears to be inevitable (e.g. Odd and Rodger (1986), Wolanski et al. (1992)). In contrast, for $C_0 = 4$ g/L and $C_0 = 10$ g/L, both the standard deviation and the range were small, owing to increased turbulent dissipation and the development of a distinct settling zone with almost homogeneous settling velocities.

Fig. 10B illustrates the influence of the time period over which particle velocities were averaged to calculate w_s and further supports the relationships described above. For $C_0 < 1$ g/L, the derived settling velocities were highly sensitive to the length of the averaging period. Extending the averaging duration reduced the scatter in the data, as random flow structures were increasingly averaged out, leaving the net settling velocity. This effect was particularly pronounced when the averaging period was increased from one minute to two minutes,

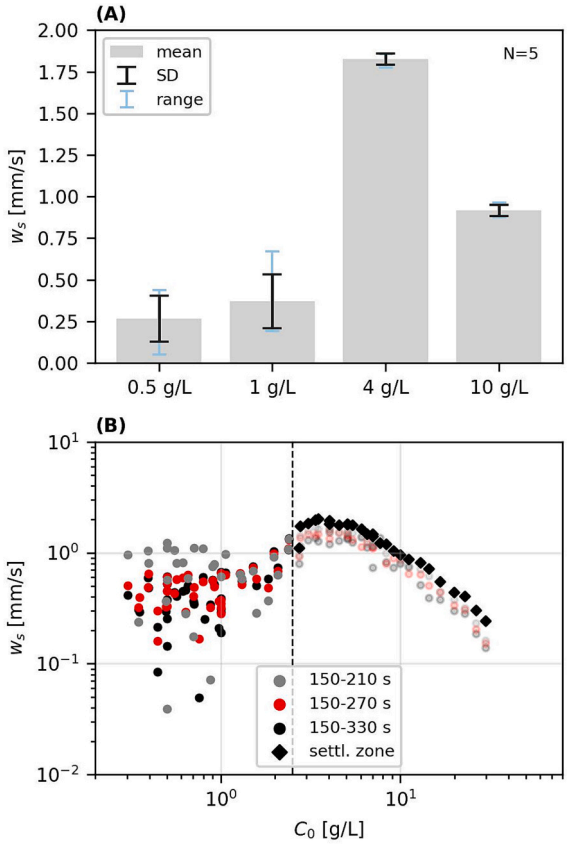

Fig. 10. A) Repeatability of UVP settling velocity measurements for four different initial sediment concentrations. The settling velocities were derived from the UVP particle velocity data following the procedure described in Section 2.4 (SD denotes the standard deviation). B) Sensitivity of the calculated settling velocities to the length of the averaging period. For $C_0 > 2.5$ g/L, black rhombuses indicate the settling velocities derived exclusively from particle velocities within the settling zone. Low-opacity markers show the settling velocities that would be obtained if the calculation were performed analogously to the $C_0 < 2.5$ g/L case.

whereas a further extension had a reduced impact. For 1 g/L $< C_0 <$ 2.5 g/L, both data scatter and sensitivity to the averaging period were reduced overall, indicating an increasing stability of the suspension within this concentration range.

For $C_0 > 2.5$ g/L, the settling velocities used in the analyses presented in the preceding sections were derived exclusively from particle velocities measured within the emerging settling zone (cf. Fig. 6D-I). In Fig. 10B, these values are shown as black rhombuses. For comparison, the low-opacity markers in this concentration range indicate the settling velocities that would be obtained if the calculation were performed analogously to the $C_0 \leq 2.5$ g/L case (averaging over a fixed column section between 10 and 48 cm depth and over the specified time period). The resulting settling velocities were generally lower than those derived from the settling zone alone, but followed the same overall trend. This reduction resulted from the inclusion of regions associated with the bed layer and the dilute suspension zone, which exhibited virtually no and partially upward-directed particle velocities, respectively.

4. Discussion

This section discusses overarching aspects of the applied methodology, the resulting limitations of the study, and implications for future research.

With the experimental setup used in this study, UVP measurements have been successfully conducted for initial sediment concentrations of up to 30 g/L. The maximum measurable sediment concentration, or equivalently the penetration depth of the ultrasound signal, could in principle be increased by raising the emitting power or the amplification level of the received backscatter. However, such adjustments may lead to saturation at the receiver stage and consequently to erroneous measurements (Signal Processing S.A., 2025). An alternative approach would be the use of a lower emitting frequency, which would increase penetration depth but reduce the spatial and velocity resolution of the measurements. Considering the measured particle velocities, the high velocity resolution required for the UVP measurements could only be achieved by limiting the maximum detectable velocity v_{max}. This led to aliasing effects in some experiments during the first 60 s of the measurements. Since this period was not used for further evaluation, this was considered acceptable. In preliminary tests, an increase of v_{max} by a factor of three was also evaluated, but this resulted in a corresponding reduction in resolution. In this configuration, aliasing could be prevented, but the calculated settling velocities showed a systematic deviation of approximately +20% compared to those derived from the lutocline curves. The measurement settings applied in this study therefore represent a compromise based on extensive preliminary testing and careful consideration of the associated trade-offs.

The experiments were conducted under laboratory conditions. Careful attention was paid to ensuring identical starting conditions and experimental procedures for all experiments. However, mixing and the associated generation of turbulence were necessary to produce a homogeneous initial suspension. After mixing ceased, the state of the suspension evolved from highly turbulent to nearly quiescent conditions. For the flocs, this implies that after extensive breakup during mixing, they subsequently grew again. The rate of floc growth depends on the frequency of interparticle collisions, that is, on sediment concentration (see Section 1). Therefore, the observed increase in settling velocity within the flocculation settling regime is presumably a time-dependent effect. This consideration also applies to field conditions, as flocs are continuously in a transitional state between breakup and growth driven by varying flow conditions. However, laboratory experiments cannot fully reproduce the genesis of flocs under natural conditions, owing to the complex and site-specific history of turbulence and concentration regimes experienced in the field. Consequently, laboratory experiments in the flocculation settling regime can only provide an approximation of settling velocities under natural conditions. Field studies, in contrast, are inherently dependent on the timing and location

of the measurements. When the initial sediment concentration corresponding to $w_{s,max}$ was reached ($C_0 = 3.5$ g/L), visual observations indicated that the flocculation process was completed within 1–2 min after the end of mixing. At even higher initial concentrations, flocculation occurred within seconds. These observations are consistent with the findings reported by Imai (1980) and Winterwerp et al. (2021). Because the influence of time diminishes in the hindered settling regime, a reasonable comparability with quiescent field conditions can be assumed. In the literature, some authors report higher settling velocities measured under field conditions compared to laboratory tests (Wolanski et al., 1992; Delo and Ockenden, 1992). This observation might be influenced by the generally high variability of settling velocities in the field (Manning and Schoellhamer, 2013) and by turbulence effects (Gratiot et al., 2005).

The flocs contained in a cohesive sediment suspension exhibit a spectrum of sizes, densities, and shapes. Consequently, characterizing the settling velocity by a single value represents a marked simplification. Often, the median settling velocity is used as a characteristic value (Pejrup and Mikkelsen, 2010; Defontaine et al., 2023). In the present study, settling velocities were derived from characteristic particle velocities v_m, which were calculated for each sampling volume as spectral-intensity-weighted averages across all velocity bins. The intensity of the received acoustic signal depends on particle size and may be further modified by flocculation processes (Ainslie, 2010; MacDonald et al., 2013). As a result, the measured power spectra, and thus the settling velocities derived from them, may be biased toward larger particles and flocs. However, the velocity spectra obtained from the UVP measurements were consistently unimodal and approximately bell-shaped when averaged over time, indicating the presence of a well-defined dominant settling velocity (cf. Fig. 4). Given that the spectra were relatively narrow and that the settling velocities derived from the UVP measurements were in good agreement with visual observations of the lutocline, the influence of this spectral weighting on the results is considered acceptable. Nevertheless, the settling velocities obtained from the UVP particle velocity data should be interpreted taking into account the limitations discussed above.

In future studies, the experimental setup could be enhanced by directly assessing the floc size evolution within the settling column. Implementing such measurements is challenging, as commonly used devices for floc size determination, such as LISST instruments or the Malvern Mastersizer, exhibit limitations with respect to maximum sediment concentration or require continuous pumping of the suspension. The latter can alter the floc size distribution due to the relatively high shear rates occurring within the tubing. Nevertheless, such measurements would provide an extended data base for interpreting the settling velocities measured by UVP and for comparison with field conditions. Applying controlled shear rates to the suspension through continuous agitation would additionally allow turbulence effects to be quantified explicitly (e.g. van Leussen (1994)). Other applications that can in principle already be realized using the current experimental setup include i) the execution of field investigations with sampling procedures comparable to Owen (1976), ii) the derivation of sediment concentration profiles from processed echo amplitude data (Meral, 2008; Pedocchi and García, 2012), and iii) the automated, high-resolution tracking of the bed level evolution in a range of laboratory experiments (cf. Fig. 8).

5. Conclusion

The aim of this study was to assess the applicability of UVP for investigating the settling process of cohesive sediments, to derive concentration-dependent settling velocities, and to evaluate and adapt common modeling approaches based on the experimental data. The results highlight both the possibilities and limitations of UVP in this context and provide a previously unavailable dataset on the settling behavior of cohesive sediments from the Port of Hamburg in the Elbe estuary. The main findings can be summarized as follows:

1. The UVP measurements allowed for a non-intrusive, high-resolution investigation of the settling process in space and time. The results revealed sediment-concentration-dependent flow patterns in the dilute suspension and the settling zone in unprecedented detail. In addition, the measurements enabled reliable identification and tracking of the lutocline, the sediment formation line, and the evolution of the bed level. Using the applied experimental setup, UVP measurements were feasible for initial sediment concentrations of up to $C_0 \cong 30$ g/L.
2. Above $C_0 \cong 2.5$ g/L, a diffuse lutocline was detectable in the visualized UVP data. With increasing initial sediment concentration, the lutocline progressively sharpened, allowing its position to be determined with a precision of one millimeter at $C_0 \cong 20$ g/L based on photographic evaluation. The settling velocities derived directly from the UVP particle velocity data and those obtained from the lutocline evolution (both the visualized UVP data and photographic analyses) showed strong agreement. These results may be interpreted as direct evidence that the settling velocity can be reliably inferred from the lutocline evolution.
3. The effective settling velocities increased approximately linearly with increasing initial sediment concentration until a maximum value of $w_{s,max} \cong 2$ mm/s was reached at $C_0 \cong 3.5$ g/L, corresponding to the flocculation settling regime. For $C_0 > 3.5$ g/L, the settling velocities exhibited an asymptotic decay for further increasing initial sediment concentrations, indicating the hindered settling regime.
4. The settling flux, calculated as $D = w_s C_0$, reached a broad maximum of $D \cong 0.01$ kg/(m^{2}s) within the range 5 g/L $< C_0 <$ 15 g/L. At higher initial sediment concentrations, the settling flux decreased, as the reduction in settling velocity outweighed the increase in sediment concentration.
5. The applied mathematical models allowed a highly accurate fit to the calculated concentration-dependent settling velocities, and the obtained fit parameters corresponded remarkably well with values reported in the literature. The behavior of the models proposed by Weilbeer (2008) and Wolanski et al. (1989) differed for concentrations close to the gelling point due to their mathematical structure. The relatively large absolute differences in the calculated settling flux within this concentration range underscore the importance of a suitable transition between settling and consolidation in higher-level numerical models.

Overall, the results demonstrate that UVP provides a robust and versatile tool for the detailed investigation of cohesive sediment settling across a wide range of concentrations. Future work should focus on extending the approach toward field applications and on coupling UVP measurements with floc size and turbulence observations to further improve parameterizations of cohesive sediment transport.

CRediT authorship contribution statement

M. Witt: Writing – original draft. **J. Patzke:** Writing – review & editing. **E. Nehlsen:** Writing – review & editing. **P. Fröhle:** Writing – review & editing.

Funding

This study was conducted as part of the research project ELMOD - "Simulation and analysis of the hydrological and morphological development of the Tidal Elbe for the period from 2013 to 2018". The project on which this report is based is funded by the German Federal Ministry of Research, Technology and Space (BMFTR) under the funding code 03F0928A. The responsibility for the content of this publication lies with the authors.

Publishing fees supported by Hamburg University of Technology (TUHH).

The authors would like to thank both institutions for the support.

Declaration of competing interest

The authors declare that they have no known competing financial interests or personal relationships that could have appeared to influence the work reported in this paper.

Data availability

Data will be made available on request.

References

Ainslie, M., 2010. Principles of Sonar Performance Modelling. Springer Berlin Heidelberg, Berlin, Heidelberg.

Dankers, P.J.T., 2006. On the Hindered Settling of Suspensions of Mud and Mud-Sand Mixtures. Dissertation. TU Delft, Delft.

Defontaine, S., Jalon-Rojas, I., Sottolichio, A., Gratiot, N., Legout, C., 2023. Settling dynamics of cohesive sediments in a highly turbid tidal river. Mar. Geol. 457, 106995. https://doi.org/10.1016/j.margeo.2023.106995.

Delo, E., Ockenden, M.C., 1992. Estuarine Muds Manual. HR Wallingford (report SR 309).

DIN, 2017. Geotechnical Investigation and Testing - Laboratory Testing of Soil - Part 4: Determination of Particle Size Distribution (ISO 17892-4:2016); German Version EN ISO 17892-4:2016. DIN-Normenausschuss Bauwesen, Berlin. https://doi.org/10.31030/2362539.

DIN, 2023. Earthworks - Chemical Tests - Part 1: Determination of Loss on Ignition; German Version EN 17685-1:2023. DIN-Normenausschuss Bauwesen, Berlin. https://doi.org/10.31030/3412786.

Gratiot, N., Michallet, H., Mory, M., 2005. On the determination of the settling flux of cohesive sediments in a turbulent fluid. J. Geophys. Res. 110 (C6), 2004JC002732. https://doi.org/10.1029/2004JC002732.

Hitomi, J., Nomura, S., Murai, Y., de Cesare, G., Tasaka, Y., Takeda, Y., et al., 2021. Measurement of the inner structure of turbidity currents by ultrasound velocity profiling. Int. J. Multiphase Flow 136, 103540. https://doi.org/10.1016/j.ijmultiphaseflow.2020.103540.

Hoskins, P.R., Martin, K., Thrush, A. (Eds.), 2010. Diagnostic Ultrasound. Physics and Equipment, Second edition. Cambridge University Press, Cambridge. https://doi.org/10.1017/CBO9780511750885.

Hunter, T.N., Peakall, J., Biggs, S.R., 2011. Ultrasonic velocimetry for the in situ characterisation of particulate settling and sedimentation. Miner. Eng. 24 (5), 416–423. https://doi.org/10.1016/j.mineng.2010.12.003.

Imai, G., 1980. Settling behavior of clay suspension. Soils Found. 20 (2), 61–77. https://doi.org/10.3208/sandf1972.20.2_61.

Imai, G., 1981. Experimental studies on sedimentation mechanism and sediment formation of clay materials. Soils Found. 21 (1), 7–20. https://doi.org/10.3208/sandf1972.21.7.

Kaveh, K., Malcherek, A., 2024. On the global parameterization of a 1DV hydromorphodynamic model of estuaries, the case of the ems estuary. Environ. Model. Softw. 179, 106125. https://doi.org/10.1016/j.envsoft.2024.106125.

Kynch, G.J., 1952. A theory of sedimentation. Trans. Faraday Soc. 48, 166–176.

LGV, 2024. Aerial photos of Hamburg. DOP Zeitreihe belaubt. Landesbetrieb Geoinformation und Vermessung (LGV), Freie und Hansestadt Hamburg. Available online at metaver.de, checked on 10/24/2025.

MacDonald, I.T., Vincent, C.E., Thorne, P.D., Moate, B.D., 2013. Acoustic scattering from a suspension of flocculated sediments. J. Geophys. Res. Oceans 118 (5), 2581–2594. https://doi.org/10.1002/jgrc.20197.

Manning, A.J., Schoellhamer, D.H., 2013. Factors controlling floc settling velocity along a longitudinal estuarine transect. Mar. Geol. 345, 266–280. https://doi.org/10.1016/j.margeo.2013.06.018.

Mantovanelli, A., Ridd, P.V., 2006. Devices to measure settling velocities of cohesive sediment aggregates: a review of the in situ technology. J. Sea Res. 56 (3), 199–226. https://doi.org/10.1016/j.seares.2006.05.002.

Mehta, A.J., 2014. An Introduction to Hydraulics of Fine Sediment Transport, 38. World Scientific Publishing Co. Pte. Ltd.. Advanced Series on Ocean Engineering.

Mehta, A.J., McAnally, W.H., 2008. Fine-grained sediment transport. In: García, M.H. (Ed.), Sedimentation Engineering. Processes, Measurements, Modeling, and Practice, 110. American Society of Civil Engineers, Reston, Va, pp. 253–306. https://doi.org/10.1061/9780784408148.CH04. ASCE manuals and reports on engineering practice.

Meral, R., 2008. Laboratory evaluation of acoustic backscatter and LISST methods for measurements of suspended sediments. Sensors (Basel, Switzerland) 8 (2), 979–993. https://doi.org/10.3390/s8020979.

Odd, N., Rodger, J.G., 1986. An Analysis of the Behaviour of Fluid Mud in Estuaries. HR Wallingford (report no SR 84).

Owen, M., 1976. Determination of the Settling Velocities of Cohesive Muds. HR Wallingford (report no. IT 161).

Papenmeier, S., 2012. Properties and dynamics of suspended load and near-bed fine cohesive sediments in highly impacted estuaries. In: Case Studies from the Weser, Ems and Elbe Estuaries (Germany). Dissertation. Christian-Albrechts Universität, Kiel.

Patzke, J., 2025. Zur Beschreibung der vertikalen Bodenaustauschprozesse von kohäsiven Sedimenten am Beispiel des Weserästuars. Dissertation. TU Hamburg, Hamburg.

Pedocchi, F., García, M.H., 2012. Acoustic measurement of suspended sediment concentration profiles in an oscillatory boundary layer. Cont. Shelf Res. 46, 87–95. https://doi.org/10.1016/j.csr.2011.05.013.

Pejrup, M., Mikkelsen, O.A., 2010. Factors controlling the field settling velocity of cohesive sediment in estuaries. Estuar. Coast. Shelf Sci. 87 (2), 177–185. https://doi.org/10.1016/j.ecss.2009.09.028.

Poelma, C., 2017. Ultrasound imaging velocimetry: a review. Exp. Fluids 58 (1). https://doi.org/10.1007/s00348-016-2283-9.

Richardson, J.F., Zaki, W.N., 1954. Sedimentation and fluidisation part 1. Chem. Eng. 32, 35–53.

Ross, M.A., 1988. Vertical Structure of Estuarine Finde Sediment Suspension. Dissertation. University of Florida.

Signal Processing S.A, 2025. DOP3000/3010 Series. User's Manual.

Takeda, Y., 1986. Velocity profile measurement by ultrasound doppler shift method. Int. J. Heat Fluid Flow 7 (4), 313–318. https://doi.org/10.1016/0142-727X(86)90011-1.

Takeda, Y., 1991. Development of an ultrasound velocity profile monitor. Nucl. Eng. Des. 126 (2), 277–284. https://doi.org/10.1016/0029-5493(91)90117-Z.

Takeda, Y., 1995. Velocity profile measurement by ultrasonic doppler method. Exp. Thermal Fluid Sci. 10 (4), 444–453. https://doi.org/10.1016/0894-1777(94)00124-Q.

te Slaa, S., 2020. Deposition and Erosion of Silt-Rich Sediment-Water Mixtures. Dissertation. TU Delft, Delft.

van Leussen, W., 1994. Estuarine Macroflocs and their Role in Fine-Grained Sediment Transport. Macrovlokken en Hun Bijdrage aan de Slibtransporten in Estuaria. Dissertation. Universiteit Utrecht, Utrecht.

van Rijn, L., Perk, L., van Maren, B., Manning, A., 2025. Particle size and settling velocity of bed and suspended sediments for mud-sand beds. Int. J. Sediment Res. 40 (2), 369–382. https://doi.org/10.1016/j.ijsrc.2024.11.007.

Weilbeer, H., 2008. Numerical simulation and analyses of sediment transport processes in the Ems-Dollard estuary with a three-dimensional model. Proc. Mar. Sci. 9, 447–462. https://doi.org/10.1016/S1568-2692(08)80032-0. Article 30.

Weilbeer, H., Winterscheid, A., Strotmann, T., Entelmann, I., Shaikh, S., Vaessen, B., 2021. Analyse der hydrologischen und morphologischen Entwicklung in der Tideelbe für den Zeitraum von 2013 bis 2018. https://doi.org/10.18171/1.089104.

Whitehouse, R.J.S., Soulsby, R.L., Spearman, J., Roberts, W., Mitchener, H.J., 2000. Dynamics of Estuarine Muds. A Manual for Practical Applications. Telford, London.

Wiklund, J., Stading, M., 2008. Application of in-line ultrasound doppler-based UVP–PD rheometry method to concentrated model and industrial suspensions. Flow Meas. Instrum. 19 (3–4), 171–179. https://doi.org/10.1016/j.flowmeasinst.2007.11.002.

Winterwerp, J.C., 1999. On the Dynamics of High-Concentrated Mud Suspensions. Dissertation. TU Delft, Delft.

Winterwerp, J.C., van Kesteren, W.G.M., 2004. Introduction to the Physics of Cohesive Sediment in the Marine Environment, 1st ed 56. Elsevier, Amsterdam. Developments in Sedimentology.

Winterwerp, J.C., van Kessel, T., van Maren, D.S., van Prooijen, B.C., 2021. Fine sediment in open water, 55. World Scientific.

Wolanski, E., Asaeda, T., Imberger, J., 1989. Mixing across a lutocline. Limnol. Oceanogr. 34 (5), 931–938. https://doi.org/10.4319/lo.1989.34.5.0931.

Wolanski, E., Gibbs, R., Ridd, P., Mehta, A., 1992. Settling of ocean-dumped dredged material, Townsville, Australia. Estuar. Coast. Shelf Sci. 35 (5), 473–489. https://doi.org/10.1016/S0272-7714(05)80026-5.

WSV, 2024. DEM (2022) of the Outer and Lower Elbe. Wasserstraßen- und Schifffahrtsverwaltung des Bundes (WSV). Available online at www.kuestendaten.de, checked on 12/16/2024.